International Journal of Mechanical, Industrial and Aerospace Sciences
ISSN: 2517-9950
Vol:6, No:4, 2012

Numerical Investigation of the Optimal Spatial Domain Discretization for the 2-D Analysis of a Darrieus Vertical-Axis Water Turbine

M. Raciti Castelli, S. De Betta and E. Benini

***Abstract*—**The optimal grid spacing and turbulence model for the 2D numerical analysis of a vertical-axis water turbine (VAWaterT) operating in a 2 m/s freestream current has been investigated. The results of five different spatial domain discretizations and two turbulence models (*k-ω SST* and *k-ε RNG*) have been compared, in order to gain the optimal y^+ parameter distribution along the blade walls during a full rotor revolution. The resulting optimal mesh has appeared to be quite similar to that obtained for the numerical analysis of a vertical-axis wind turbine.

***Keywords* —** CFD, vertical axis water turbine, NACA 0025, blade y^+.

I. Introduction and Background

CONVENTIONAL hydroelectricity, considered as one of the dominant forms of green Energy, is facing a scarcity of suitable installation sites, just as the need for renewables is becoming greater. Therefore, alternative forms of hydropower must be pursued, in order to tap the hydroelectric energy potential of the world. Kinetic hydropower, using submerged turbines in existing currents to produce electricity, is one of such alternatives. A kinetic hydropower turbine doesn't require large infrastructures, such as dams and powerhouses, thus reducing both cost and deployment time. Moreover, with no reservoir or spillways, the resulting environmental impact is minimal [1].

The process of hydrokinetic energy conversion implies the use of river (or other man-made waterways) streams and tidal currents for the generation of electricity. This emerging class of renewable technology is being strongly recognized as a unique and unconventional solution that falls within the realms of both in-land water resource and marine energy [2].

For the technical development of water turbines, much can be learned from wind turbines, even if different operating boundary conditions, such as fluid density and kinematic viscosity, must be taken into account. Moreover, since the operating fluid is water, cavitation can eventually occur. Besides, the main advantage of the troposkien-shaped blades on a wind turbine is the great reduction of bending moments.

Marco Raciti Castelli is a Research Associate at the Department of Mechanical Engineering of the University of Padua, Via Venezia 1, 35131 Padova, Italy (e-mail: marco.raciticastelli@unipd.it).

Stefano De Betta has completed his M.Sc. in Aerospace Engineering at the University of Padua, Via Venezia 1, 35131 Padova, Italy.

Ernesto Benini is an Associate Professor at the Department of Mechanical Engineering of the University of Padua, Via Venezia 1, 35131 Padova, Italy (e-mail: ernesto.benini@unipd.it).

Unfortunately, this advantage is largely lost in water, because water dynamic forces on rotor blades typically exceed centrifugal forces, determining a high buckling risk during blade upstream pass [3].

A great advantage of ocean and tidal currents is connected to its highly predictable power output. Apart from that, energy extraction from unregulated watercourses has very much in common with wind power, the main difference being the density of water, which is approximately 800 times the density of air. This means that a turbine for underwater applications can be much smaller than an air turbine of the same rated power [4].

One commonly used hydro-kinetic turbine is the Darrieus rotor, originally patented as wind turbine in the USA in 1931 by G. J. M. Darrieus [5]. Darrieus' patent employed a set of curved blades approximating the shape of a perfectly flexible cable, namely the Troposkien shape. Later, vertical axis designs, comprising straight bladed architectures, appeared under different names, such as "H-Darrieus" or "Squirrek Cage Darrieus" turbines [6].

The behavior of a vertical axis Darrieus wind or water turbine is characterized by the influence of dynamic stall and also by a highly turbulent flow: since turbulence plays a dominant role in the transport of mean momentum and other parameters, it is necessary to properly resolve turbulence quantities, in order to achieve an acceptable accuracy in the numerical predictions. In fact, due to the strong interaction of mean flow and turbulence, the numerical results for turbulent flows tend to be more susceptible to grid dependency than those for laminar flows. The numerical marker adopted to control the grid dimension close to rotor blades is the y^+ parameter: it consists of a mesh-dependent dimensionless distance that quantifies the degree of wall layer resolution, in formulas:

$$y^+ = \rho \cdot u_t \cdot y / \mu \quad (1)$$

where ρ is water density, u_t is the friction velocity, y the cell distance from the blade profile and μ is the dynamic viscosity of water.

In the present work, 2D numerical simulations of a four-bladed Darrieus VAWaterT were performed. Five different spatial grid resolutions were investigated. For every tested mesh, both average and maximum y^+ were analyzed, in order to determine the optimal grid configuration and thus obtaining the best resolution of the numerical flow field.

II. Model Geometry

The main geometrical features of the analyzed rotor are summarized in Table I.

TABLE I
MAIN GEOMETRICAL FEATURES OF THE ANALYZED ROTOR

Denomination	Value
Drotor [mm]	1030
Hrotor [mm]	1 (2D simulation)
Blade profile	NACA 0025
c [mm]	85.8
N [-]	4

Rotor azimuthal position was identified by the angular coordinate of blade No. 1 centre of pressure (located at 25% of the chord for a NACA 0025 blade profile), starting between the 2nd and 3rd Cartesian plane octants, as can be seen from Fig. 1. The main dimensions of the computational domain are shown in Fig. 2.

In order to obtain a fully development of the wake, Ferreira et al. [7] placed inlet and outlet boundary conditions respectively 10 diameters upstream and 14 diameters downstream with respect to rotor test section for a wind tunnel CFD simulation. Beri and Yao [8] placed the inlet condition only 3 diameters upwind with respect to rotor test section, while Shiono et al. [9] adopted a 100 rotor diameter length and 10 diameters width thank. In the present work, because of the huge domain width necessary to avoid solid blockage, inlet and outlet were placed respectively 37 rotor diameters upstream and 60 rotor diameters downstream with respect to the test section.

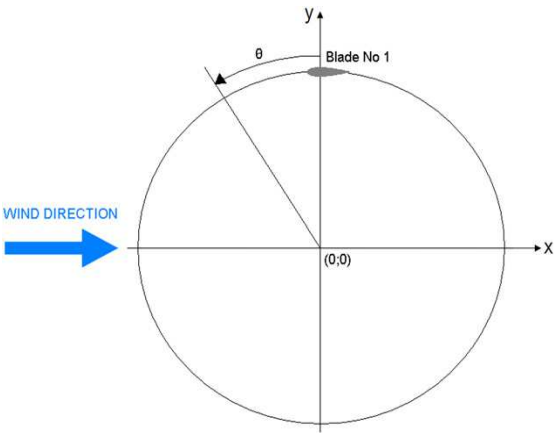

Fig. 1 Rotor azimuthal position, identified by the azimuthal coordinate of the centre of pressure of blade No. 1

As the aim of the present work was to reproduce the operation of a rotating machine, the use of moving sub-grids became necessary. In particular, the discretization of the computational domain into macro-areas led to two distinct sub-grids:

- a rectangular outer zone, determining the overall calculation domain, with a circular opening centered on the turbine rotational axis, which was identified as *Water Tank sub-grid*, fixed;
- a circular inner zone, which was identified as *Rotor sub-grid*, revolving with rotor angular velocity ω.

Inlet boundary condition was set as a *velocity inlet*, with a constant velocity profile of 2 m/s, while outlet was set as a *pressure outlet*. Two *symmetry* boundary conditions were used for the two side walls. The circumference around the circular opening, centered on the turbine rotational axis, was set as an *interface*, thus ensuring the continuity in the flow field.

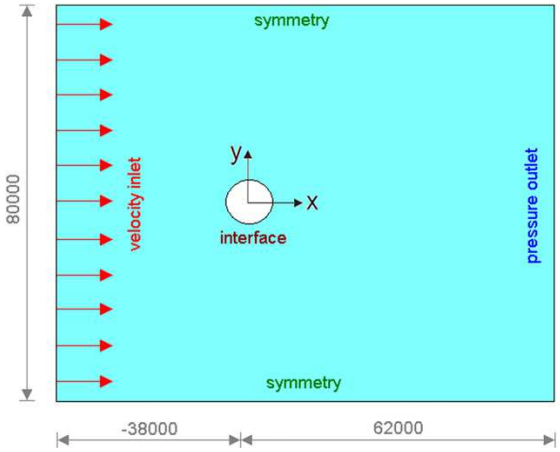

Fig. 2 Main dimensions [mm] of the computational domain

The fluid area simulating the revolution of the water turbine was defined as *Rotor sub-grid* and was characterized by a moving mesh, rotating at the same angular velocity of the turbine. Its location coincided exactly with the circular opening inside the *Water Tank sub-grid* area and was centered on the turbine rotational axis. Fig. 3 shows the main dimensions and the boundary conditions of the *Rotor sub-grid* area.

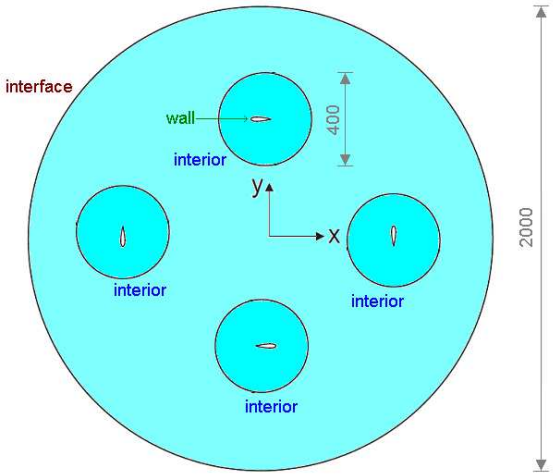

Fig. 3 Schema of the rotor sub-grid area for a three-bladed VAWaterT (dimensions in mm)

All blade profiles inside the *rotor sub-grid* area were enclosed in a control circle of 400 mm diameter: this geometry had no physical significance, being its aim to allow a precise

dimensional control of the grid elements in the area close to the rotor blades, by adopting a first size function operating from the blade profile to the control circle itself and a second size function operating from the control circle to the whole *Rotor sub-grid* area, ending with grid elements of the same size of the corresponding *Water Tank sub-grid* elements. An *interior* boundary condition was used for control circle borders, thus ensuring the continuity of the cells on both sides of the mesh.

A sliding mesh was adopted in order to reproduce the rotational motion of the VAWaterT. To discretize the flow field, an unstructured grid was chosen for the whole computational domain, in order to reduce the engineering time to prepare the CFD simulations. The mesh on both sides of the *interface* (*Rotor sub-grid* and *Water Tank sub-grid* areas) had approximately the same characteristic cell size, in order to obtain faster convergence [10].

An isotropic unstructured mesh was chosen for the *Rotor sub-grid*, in order to guarantee the same accuracy in the prediction of rotor's performance during the revolution of the turbine (according to the studies of Commings et al. [11]) and also in order to test the prediction capability of a very simple grid. Considering their features of flexibility and adaption capability, unstructured meshes are in fact very easy to obtain, for complex geometries, too, and often represent the "first attempt" in order to get a quick response from the CFD in engineering work. The *Rotor sub-grid* mesh is represented in Fig. 4.

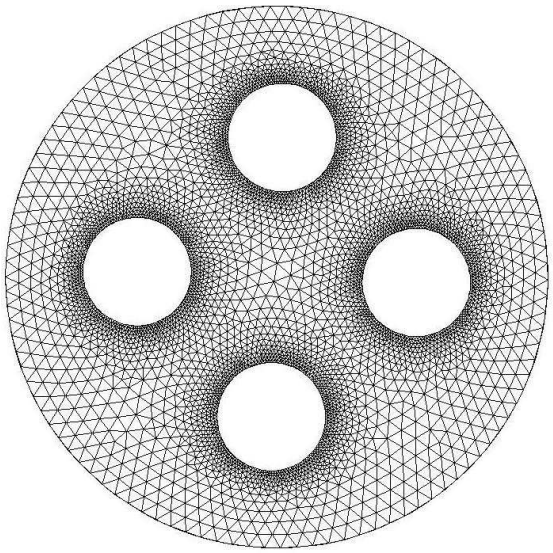

Fig. 4 View of the *Rotor sub-grid* mesh

Being the area close to the blade profiles, great attention was placed in the control circle. The computational grids were constructed from lower topologies to higher ones, adopting appropriate size functions, in order to cluster grid points near the leading edge and the trailing edge of the blade profile, so as to improve the CFD code capability of determining lift, drag and the separation of the flow from the blade itself. All the differences between the various meshes adopted in the present work were concentrated in this area.

Three size functions were adopted inside the control circle, as shown in Fig. 5:

- size function No. 1 started from the leading edge and influenced both inner and outer blade profile;
- size function No. 2 started from the trailing edge and influenced both inner and outer blade profile;
- size function No. 3 started from the blade profile and influenced the whole *control circle* area.

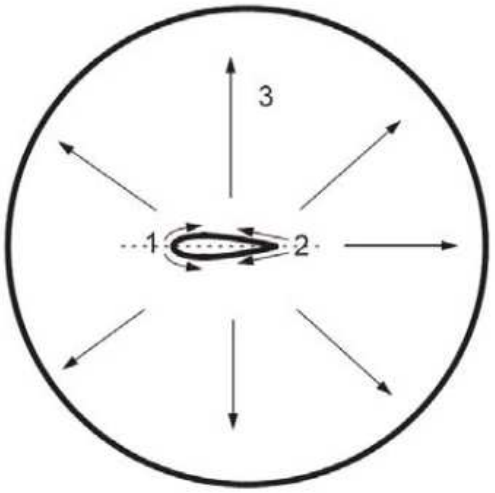

Fig. 5 Schema of the size functions applied to the main control circle elements

III. Temporal Discretization and Convergence Criteria

The commercial CFD package adopted for the proposed numerical computations was Fluent 6.3.26, which implements 2-D Reynolds-averaged Navier-Stokes equations using a finite volume based solver. The fluid was assumed to be incompressible.

As a global convergence criterion, each simulation was run until the difference between two following periods of revolution, corresponding to a rotation of 90° due to rotor four-bladed geometry, was lower than 1%. Residuals convergence criterion for each single time step was set to 10^{-5}.

The simulations, performed on a 2.33 GHz clock frequency quad core CPU with Hyper-Threading, were run until the instantaneous torque values showed a deviation of less than 1% compared with the corresponding values of the previous period. Total computational time was about 2 hours for each simulation.

IV. Wall y^+ Strategy

All the analysis performed in this work aimed at the determination of the optimum value of the y^+ parameter, as a guidance in selecting the appropriate grid configuration and corresponding turbulence models, according to the numerical strategy proposed by Raciti Castelli et al. [12].

The CFD analysis of a Darrieus water turbine shows some peculiar characteristics that make the control of the y^+ parameter quite difficult. The flow field around the rotor is in fact characterized by huge unsteadiness, due to the continuous variation of the angle of incidence on the blade profile, as can be seen from Figs. 6 and 7. Moreover, the y^+ parameter varies with the tip speed ratio, as can be seen from Fig. 8, so the subsequent considerations about the y^+ were made considering the tip speed ratio that produces the higher power output, i.e. $\lambda = 2.43$.

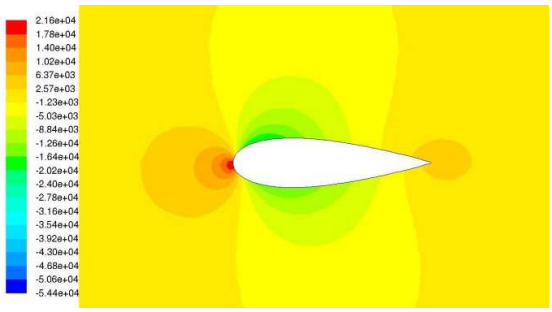

Fig. 6 Contours of static pressure [Pa] close to rotor blade No. 1 (θ=0°, λ=2.43)

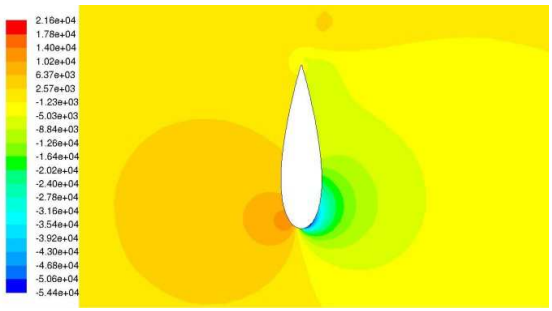

Fig. 7 Contours of static pressure [Pa] close to rotor blade No. 1 (θ=90°, λ=2.43)

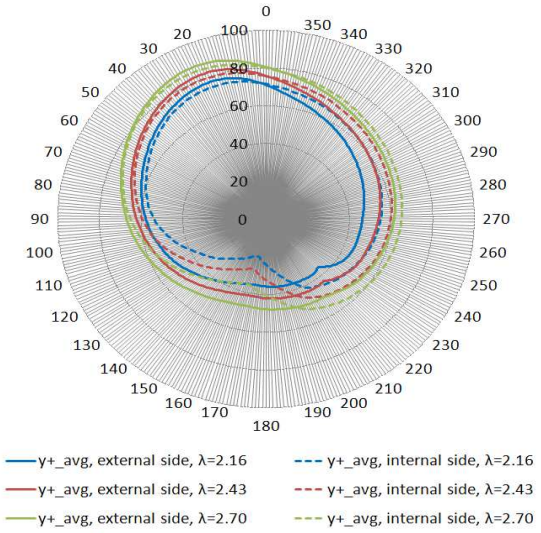

Fig. 8 Evolution of the average y^+ parameter along both the internal and external sides of rotor blade, for a full rotation of blade No. 1 and for different values of the tip speed ratio (MOD3.5 mesh)

It can be noted that, varying the tip speed ratio, the shape of the average y^+ (for the same mesh, over an entire revolution) remains the same.

Depending on the boundary layer analysis settings, the following y^+ values are required [10]:

- $30 < y^+ < 300$ for wall function based simulations, when the mesh is only fine enough to resolve up to the turbulent region ($y^+ > 30$). Values close to 30 are highly desirable;
- $1 < y^+ < 5$ for fine enough meshes to resolve the laminar sub-layer.

TABLE II
MAIN FEATURES OF THE FIVE TESTED GRIDS

	MOD 1	MOD 2	MOD 3	MOD 3.5	MOD 4
Starting grid size from airfoil leading edge [mm]	1.30	1.00	0.50	0.40	0.25
Growth factor from airfoil leading edge [-]	1.08	1.08	1.08	1.08	1.08
Starting grid size from airfoil trailing edge [mm]	0.40	0.40	0.40	0.35	0.20
Growth factor from airfoil trailing edge [-]	1.28	1.28	1.28	1.28	1.28
Maximum grid size on airfoil [mm]	3.50	2.00	1.00	0.75	0.50
Growth factor from airfoil surface to *Rotor sub-grid* area [-]	1.25	1.25	1.25	1.25	1.25
Maximum grid size on *Rotor sub-grid* area [mm]	10	10	10	10	10

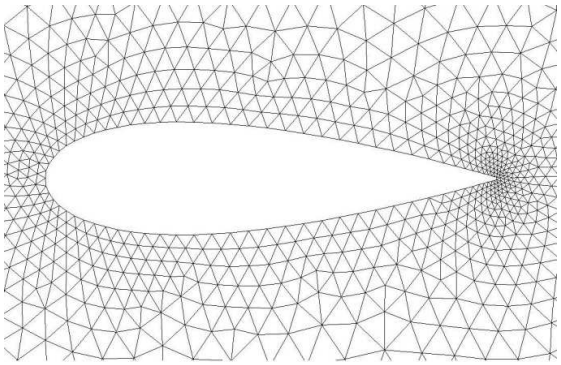

Fig. 9 MOD1 mesh

While for stationary numerical simulations the values of y^+ are only space-depending, in non-stationary computations, such as in the case of a VAWaterT, the y^+ is also time-dependent. This time-dependence is explicated by the position of the blades. As a result, the y^+ parameter is a function of both rotor angular velocity and blade azimuthal coordinate, in formulas:

$$y^+ = f(\omega; \theta) \quad (2)$$

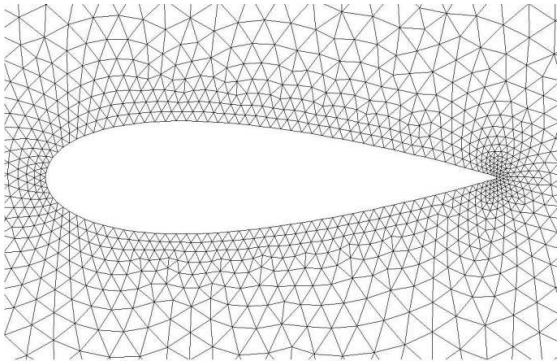

Fig. 10 MOD2 mesh

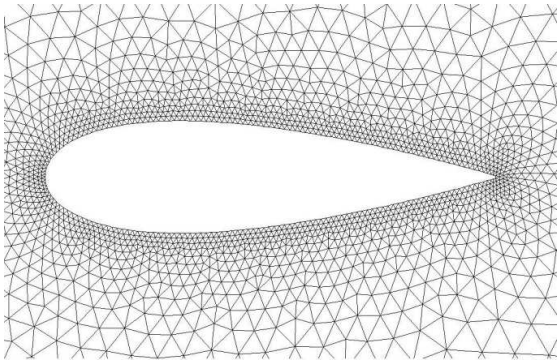

Fig. 11 MOD3 mesh

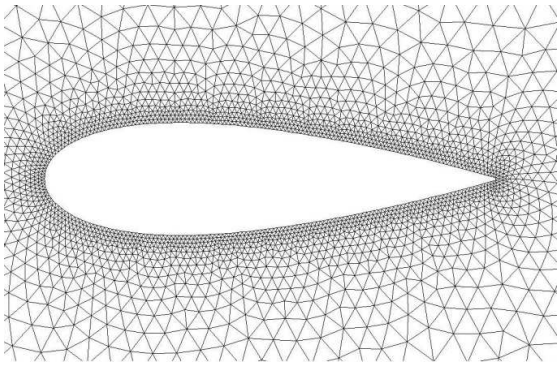

Fig. 12 MOD3.5 mesh

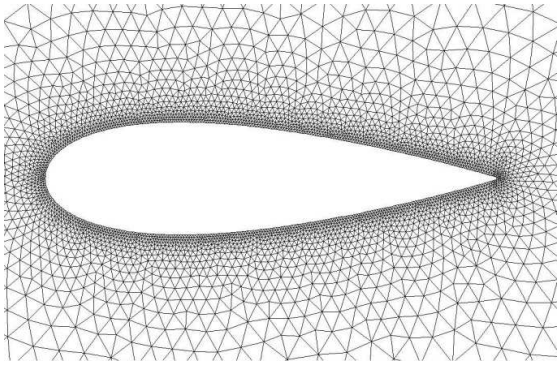

Fig. 13 MOD 4 mesh

Also y^+ maximum values are considered in this work, in order not to exceed the limit value of 100. The minimum values of the parameter don't offer significant information, because the flow velocity near stagnation points tends to zero. Nevertheless, it's important for the y^+ parameter not to descend below 30 for large zones of the blade profile.

In order to test the code sensitivity to the number of grid points, five unstructured meshes were adopted for the *Rotor Sub-Grid*, while the *Water Tank Sub-Grid* remained substantially the same. The main features of the five tested meshes are summarized in Table II.

Figs. from 9 to 13 show a comparison between the five adopted spatial grid discretizations. A significant decrease of the wall cell size can be clearly seen passing from MOD1 mesh to MOD4 mesh.

V. Turbulence Model Selection

Several works concerning the simulation of the flow field around 2D VAWTs were based on the one-equation *Spalart-Almaras* (S-A) and the two-equations *k-ε* model [13] [14] [15] [16] [17]. Ferreira et al. [7] proved that these two models are unable to properly predict the large eddies at high angles of attack. Also Wolfe and Ohcs [18] showed that *Standard k-ε* could determine inaccurate results after flow separation. However, Howel et al. [19] observed that the *RNG k-ε* model can predict flow fields involving large flow separations more accurately than standard *k-ε*.

As observed by Yu et al. [20], for airfoil flows with great adverse pressure gradient and separation, the choice of a turbulence model is very important: the *k-ω SST* turbulence model can achieve good results because of its capability of capturing the main flow-field characteristics in the near wall layers and separated flow regions. In the case of low Reynolds number, which is typical for wind turbine airfoil flows, laminar-to-turbulent transition is also an important factor that should be taken into account, in order to more accurately predict flow separation and skin friction drag.

k-ω SST turbulence model was chosen for the present work, because of its good capability to describe flow separation [21] [22] [23] which occurs in flow fields dominated by adverse pressure gradients, even if it has shown a certain sensitivity to grid size [24]. The *k-ω SST* is an enhancement of the *Standard k-ω* because it presents [10]:

- gradual change from the *Standard k-ω* model in the inner region of the boundary layer to a high-Reynolds-number version of the *k-ε* model in the outer part of the boundary layer;
- modified turbulent viscosity formulation to account for the transport effects of the principal turbulent shear stress.

Also the *RNG k-ε* model with standard wall function was utilized as a comparison with the results obtained with the *k-ω SST* turbulence model.

VI. Results and Discussion

A complete campaign of simulations, based on full RANS unsteady calculations, was performed with the aim of determining the optimal spatial grid resolution, as far as the y^+ distribution is concerned.

The tip speed ratio, defined as:

$$\lambda = \omega \cdot R_{rotor} / V_{\infty} \quad (3)$$

was varied from a value of λ=0.54 (which corresponds to an angular velocity of ω=2.1 rad/s for an incoming freestream current of 2 m/s) to λ=3.24 (which corresponds to an angular velocity of ω=12.6 rad/s). These conditions correspond to a range of blade Reynolds numbers, defined as:

$$Re = \rho \cdot R_{rotor} \cdot \omega \cdot c / \mu \quad (4)$$

varying from $9.25 \cdot 10^4$ to $5.55 \cdot 10^5$. The dynamic viscosity μ was assumed to be 0.001 Pa·s and the density ρ was set to 1000 kg/m^3.

Fig. 14 presents the comparison between the average y^+ parameter obtained using the five grid spacings described in the previous section for λ=2.43. It can be clearly seen that the average y^+ parameter over a revolution presents a common trend with respect to the different meshes. For instance, the decrease of the y^+ for the internal side of the airfoil, registered during the upstream part of blade revolution for θ=140°, can be noticed for all the examined grids, as evidenced by the red circle.

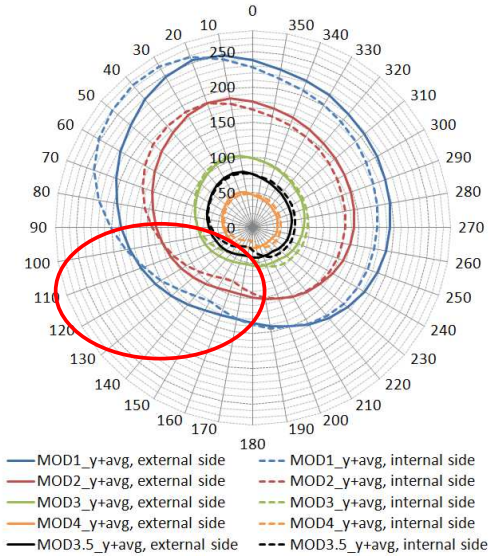

Fig. 14 Average values of y^+ for the five adopted grid spacings (λ=2.43)

From Fig. 14 it seems that the only acceptable values of the average y^+ are obtained with MOD3.5 mesh. MOD1, MOD2, and MOD3 grids present y^+ values greater than 100, while MOD4 grid presents average values of y^+ below the limit of 30, in particular in the post-stall phase. This observation lead to the discharging of such grids. Fig. 15 represents a close-up on the average and maximum values of MOD3.5 mesh. It can be noticed that the average values of y^+ are included in the interval from 30 to 80, approaching 30 only for the azimuthal position of about 160° and just for a few degrees. The maximum values sometimes exceed 100, but a finer mesh would lead to values of y^+ lower than 30 for a too large zone during a full blade revolution.

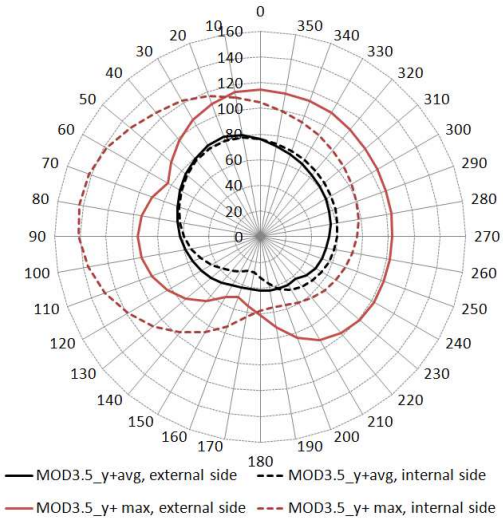

Fig. 15 Average and maximum values of y^+ for MOD3.5 and λ=2.43

TABLE III
PEAK POWER COEFFICIENT PERCENTAGE DEVIATIONS WITH RESPECT TO MOD3.5 GRID

Mesh type	C_p (λ=2.43) [-]	ΔC_p [%]
MOD3.5	0.30	-
MOD1	0.35	16.7
MOD2	0.35	16.7
MOD3	0.33	10.0
MOD4	0.22	-26.7

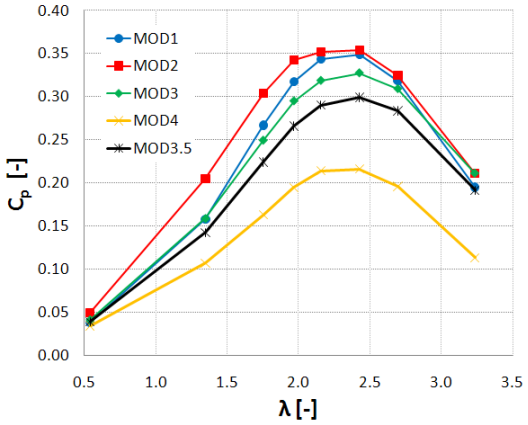

Fig. 16 Power curves obtained with the five tested grids as a function of the tip speed ratio

Fig. 16 shows the values of power coefficient, defined as:

$$C_p = P / (\tfrac{1}{2} \cdot \rho \cdot A_s \cdot V_{\infty}^3) \quad (5)$$

obtained for the five analyzed grids at different tip speed ratios. As can be clearly seen, the results are not grid

independent, as expected choosing the *k-ω SST* turbulence model. The percentile differences in peak power coefficient with respect to the MOD3.5 grid, are summarized in Table III.

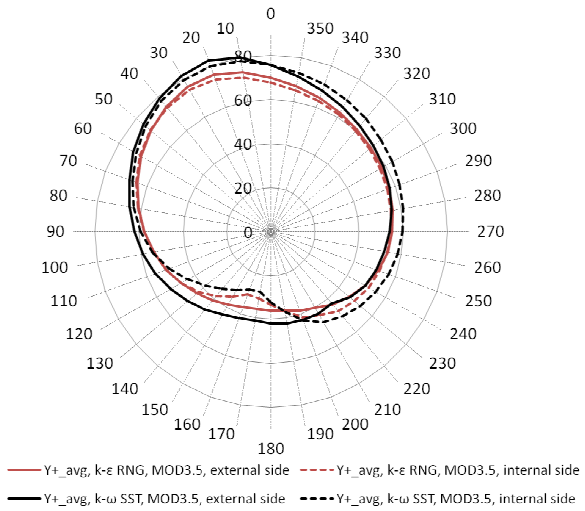

Fig. 17 Average y^+ parameter obtained with *k-ε RNG* and *k-ω SST* turbulence models, MOD3.5 mesh

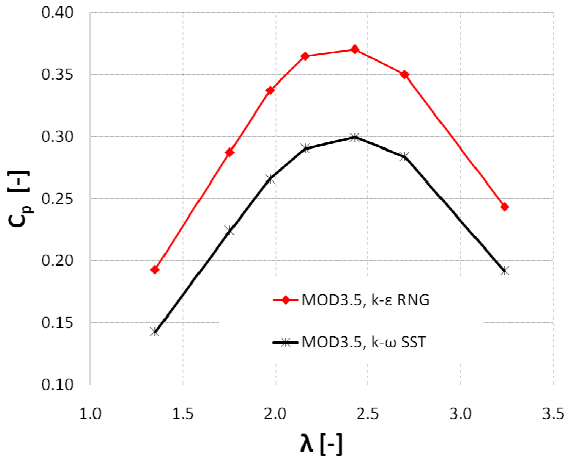

Fig. 18 Comparison between the computed powercurves for both *k-ε RNG* and *k-ω SST* turbulence models, MOD3.5 grid

Due to the lack of literature data, the computed powercurves couldn't be compared with experimental results, so a definitive validation was not possible. Nevertheless, the fact that the numerically predicted powercurves reproduce approximately the same shape and, more important, the fact that peak power coefficients are characterized by the same tip speed ratio, (i.e. λ=2.43), can be assumed as a clue of the adoption of a proper spatial resolution. Besides, Raciti Castelli et al. [12] proved that, through an accurate near-blade y^+ strategy, it is possible to correctly replicate the shape of the experimental rotor power curve, being the numerical code able to capture the tip speed ratio of maximum power coefficient.

In order to investigate the influence of the turbulence model on the prediction capabilities of the numerical code, the simulations were performed also adopting the *k-ε RNG* turbulence model. The results are presented in Fig. 17: it can be clearly seen that the values of y^+ during the revolution are not coincident, because the y^+ does not depend only on the grid size, but also by other parameters that are solution-dependent.

Fig. 18 shows a comparison between the curves of power coefficient as a function of the tip speed ratio for both adopted turbulence models: it can be seen that the *k-ε RNG* over-predict the power output, but the shape of the curve is substantially the same. For the *k-ε RNG* model, some simulations were done using the MOD3 grid, finding that the predictions in terms of C_p resulted substantially the same of that obtained with MOD3.5, confirming the low grid sensitivity of *k-ε* models family.

VII. Conclusions and Future Works

Five different grid spacings were analyzed in order to find the optimal spatial discretization based on the y^+ parameter as an indicator of the quality of the near-blade mesh for a 2D vertical-axis water turbine simulation.

The choice of turbulence model, based on literature data, led to *k-ω SST*. Due to the unsteadiness of the characteristics of the flow field, as the angle of attack, a direct evaluation of the y^+ resulted impossible. For this reason, a statistical analysis on the y^+ parameter was performed, in order to determine the optimal spatial grid distribution. The resulting optimal mesh appeared to be quite similar to that obtained by Raciti Castelli et al. [12] for a vertical-axis wind turbine.

In order to investigate the influence of the turbulence model on the prediction capabilities of the numerical code, another turbulence model widely used in literature, the *k-ε RNG*, was tested: this model over-predicted the results of the *k-ω SST*, but the shape of the power curve resulted the same, as well as the optimal value of the tip speed ratio.

Future works should focus on the development of water tank measurements, to definitively validate the proposed numerical simulations.

Acknowledgements

The present work was developed in cooperation with Vortex Energy S.r.l. (Italy), as a part of a research project finalized to the manufacturing of a Darrieus VAWaterT.

Nomenclature

A_s [m^2]	rotor swept area
c [m]	chord length
C_p [-]	water turbine power coefficient
D_{rotor} [m]	rotor diameter
H_{rotor} [m]	rotor height
N [-]	rotor blade number
P [W]	water turbine power output
Re [-]	Reynolds number
R_{rotor} [m]	rotor radius
u_t [m/s]	friction velocity
V_∞ [m/s]	free water velocity

y [m]	cell distance from the blade profile
y^+ [-]	y_{plus} parameter
θ [°]	blade No. 1 azimuthal position
λ [-]	tip speed ratio
μ [Pa·s]	dynamic viscosity
ρ [kg/m^3]	water density
ω [rad/s]	rotor angular velocity

REFERENCES

[1] D.L.F. Gaden and E.L. Bibeau, "A numerical investigation into the effect of diffusers on the performance of hydro kinetic turbines using a validated momentum source turbine", *Journal of Renewable Energy* 35, pp. 1152-1158, 2010.

[2] M. J. Khan, G. Bhuyan, M.T. Iqbal and J.E. Quaicoe, "Hydrokinetic energy conversion systems and assessment of horizontal and vertical axis turbines for river and tidal applications: A technology status review", *Journal of Applied Energy* 86, pp. 1823-1835, 2009.

[3] Kirke B. K. and Lazauskas L., "Limitations of fixed pitch Darrieus hydrokinetic turbines and the challenge of variable pitch", *Renevable Energy* 36 pp. 893-897, 2011.

[4] S. Bernard, A. Georgescu, S. C. Georgescu, R. Susan-Resiga and I. Anton, "*Flow Investigation in Achard Turbine*", Proceedings of the Romanian Academy, Series A, Vol. 9, Number 2/2008.

[5] G. J. M. Darrieus, "Turbine having its Rotating Shaft Transverse to the Flow of the Current", *U.S. Patent No. 1,835,018*, issued on Dec. 8, 1931.

[6] M. J. Khan, M. T. Iqbal and J. E. Quaicoe, "Design Considerations of a Straight Bladed Darrieus Rotor for River Current Turbines", *IEEE International Symposium on Industrial Electronics*, Montreal (Quebec), 9-13 July, 2006.

[7] S. Ferreira, H., Bijl, G. van Bussel and G. van Kuik, "Simulating dynamic stall in a 2D VAWT: modeling strategy, verification and validation with particle image velocimetry data", *Journal of Physics*: Conference Series 75 (2007), 012023.

[8] H. Beri and Y. Yao, "Computational Analysis of Vertical Axis Wind Turbine with Open-Able Airfoil, *Asia-Pacific Power and Energy Engineering Conference* (APPEEC), Wuhan (China), 25-28 March, 2011.

[9] M. Shiono, K. Suzuki, S. Kiho, "Output Characteristics of Darrieus Water Turbine with Helical Blades for Tidal Current Generations", 12th International Offshore and Polar Engineering Conference, Kitakyush (Japan), 26-31 May 2002.

[10] Fluent Inc., *Fluent User's Manual*, 2006.

[11] R. M. Cummings, J. R. Forsythe, S. A. Morton and K. D. Squires, "Computational challenges in high angle of attack flow prediction", *Progress in Aerospace Sciences*, Vol. 39, No. 5. (July 2003), pp. 369-384.

[12] M. Raciti Castelli, G. Ardizzon, L. Battisti, E. Benini, G. Pavesi, "Modeling Strategy and Numerical Validation for a Darrieus Vertical Axis Micro-Wind Turbine", *ASME 2010 International Mechanical Engineering Congress & Exposition*, November 12-18, 2010, Vancouver (British Columbia), IMECE2010-39548.

[13] M. O. L. Hansen and D. N. Soresen, "CFD model for Vertical Axis Wind Turbine", *European Wind Energy Conference*, Copenhagen (Denmark), 2-6 July 2001.

[14] A. Allet, S. Hallè and I. Paraschivoiu, "Numerical simulation of dynamic stall around an airfoil in Darrieus motion", *Journal of Solar Energy Engineering*, 121, pp. 69-79, February 1999.

[15] I. Paraschivoiu and A. Allet, "Aerodynamic analysis of the Darrieus wind turbines including dynamic-stall effects", Journal of Propulsion and Power 4, pp. 472-477, 1988.

[16] I. Paraschivoiu and C. Béguier, "Visualization, measurements and calculations of dynamic stall for a similar motion of VAWT", *Proceedings of the European Wind Energy Conference*, Herning (Denmark), 1998.

[17] I. Paraschivoiu, *Wind Turbine Design – With Emphasis on Darrieus Concept*, Polytechnic international Press, 2002.

[18] E. P. Wolfe and S. S. Ochs, "CFD calculations of S809 aerodynamic characteristics", *AIAA Aerospace Sciences Meeting, 1997*, AIAA paper 97-0973.

[19] R. Howell, N. Qin, J. Edwards and N. Durrani, "Wind tunnel and numerical study of a small vertical axis wind turbine", *Journal of Renewable Energy* 35 pp. 412-422, 2010.

[20] G. H. Yu, X. C. Zhu and Z. H. Du, "Numerical simulation of a wind turbine airfoil: dynamic stall and comparison with experiments", *Power and Energy Journal*, Vol. 224, 2010.

[21] P. R. Spalart, "A One-Equation Turbulence Model for Aerodynamic Flows", *La Recherche Aerospatiale*, 1994.

[22] F. R. Menter, "Two-Equation Eddy-Viscosity Turbulence Models for Engineering Applications", *AIAA Journal* 32 (8), 1994.

[23] D. C. Wilcox, "Turbulence Modeling for CFD", *DCW Industries Inc.*, La Canada (California), 1998.

[24] J. E. Bardina, P. G. Huang and T. J. Coakley, "Turbulence Modeling Validation, Testing and Development", *Technical Report 110446*, NASA, 1997.